International Journal of Mass Spectrometry 297 (2010) 55–62

Contents lists available at ScienceDirect

International Journal of Mass Spectrometry

journal homepage: www.elsevier.com/locate/ijms

Infrared spectra and structures of diamantyl and triamantyl carbocations

Olivier Pirali[a,b,*], Héctor Alvaro Galué[c], Jeremy E. Dahl[d], Robert M.K. Carlson[d], Jos Oomens[c,e,**]

[a] Laboratoire de Photophysique Moléculaire, CNRS, Université Paris-Sud, 91405 Orsay Cedex, France
[b] Synchrotron SOLEIL, L'Orme des Merisiers Saint-Aubin, 91192 Gif-sur-Yvette, France
[c] FOM-Institute for Plasma Physics Rijnhuizen, Edisonbaan 14, 3439MN Nieuwegein, The Netherlands
[d] MolecularDiamond Technologies, Chevron-Technology Ventures, 100 Chevron Way, Richmond, CA 94802, United States
[e] Van't Hoff Institute for Molecular Sciences, University of Amsterdam, Amsterdam, The Netherlands

ARTICLE INFO

Article history:
Received 9 March 2010
Received in revised form 7 May 2010
Accepted 13 May 2010
Available online 27 May 2010

Keywords:
Diamondoid molecule
Diamantane
Triamantane
IR spectroscopy
Carbocation
Astrochemistry

ABSTRACT

Gas-phase infrared spectra have been recorded for the diamantyl and triamantyl carbocations by infrared multiple photon dissociation (IRMPD) spectroscopy using the free electron laser FELIX. Chemical ionization of the neutral parent diamondoid molecule in an rf ion trap is accompanied by H-atom loss, forming a stable closed-shell carbocation. Comparing the IRMPD spectra with harmonic DFT calculations permits to determine the structures of the species trapped in our set-up. Comparison of experimental and calculated spectra suggests that H-atom abstraction occurs on a tertiary carbon (CH group) rather than on a secondary carbon (CH_2 group), as also indicated by the calculated relative energies of the various isomers. Combining experimental results and DFT calculations, we compare the spectra of neutral and carbocationic forms of adamantane, diamantane and triamantane. Substantial differences are observed between the IR spectra of neutral and ionic species. In the ions, the 3 μm CH stretching modes become much weaker, while the other mid-IR modes strongly gain in intensity. An intense band centered at 1200 cm^{-1} due to a CH/CH_2 bending mode appears to be characteristic of the dehydrogenated cationic species. Finally, the intensities of the low frequency modes ($\leq$ 900 cm^{-1}) associated with carbon cage deformations appear to be most sensitive to the ionization and dehydrogenation state of the molecules.

1. Introduction

Diamondoid molecules consist of a cubic-diamond carbon framework, where all carbon atoms are sp^3 hybridized and dangling bonds on the periphery are terminated with hydrogen. Adamantane ($C_{10}H_{16}$), which consists of one diamond cage, has been first synthesized by Prelog and Seiwerth [1], but a much more efficient synthesis was discovered by von Rague-Schleyer [2]. Diamantane ($C_{14}H_{20}$) and triamantane ($C_{18}H_{24}$) consist of 2 and 3 face-fused diamond cages, respectively. Like adamantane, they can be synthesized in solution by carbocation-mediated thermodynamically controlled equilibration reactions [3]. Higher diamondoids cannot be synthesized by these methods [4,5]. Recently, Dahl et al. [6] succeeded in isolating pure samples of higher diamondoid molecules from crude oil [7]. The samples isolated range from adamantane to undecamantane and permit the study of the spectra and structures of this family of molecules.

Due to their remarkably high stability, the presence of diamond-like species in different regions of space has been hypothesized for several decades (see e.g., Saslaw and Gaustad [8]). In 1987 Lewis et al. [9] reported the first extraction of nanometer-sized diamonds from meteorites supporting the suggested presence of these molecules in the interstellar medium (ISM). Furthermore, two broad emission features centered at 3.43 μm and 3.53 μm (about 2830 cm^{-1} and 2915 cm^{-1}) observed towards two Herbig stars, HD97048 and Elias 1, have been attributed to large gas-phase diamondoid molecules or nanoparticles [10]. In addition, a broad absorption feature observed towards several sources at 3.47 μm (2880 cm^{-1}) has been suggested to indicate the presence of these molecules in ices present in dense clouds [11]. However, other assignments for this feature have also been proposed [12] and these are now considered to be more likely.

While it was originally considered that only diamondoid nanocrystals larger than about 50 nm could be the carriers of the two emission features at 3.43 μm and 3.53 μm [13–15], the IR spectra of molecular diamondoid species revealed that these much smaller *higher diamondoids* could also be responsible for the two emission features [16].

* Corresponding author at: Laboratoire de Photophysique Moléculaire, CNRS, Université Paris-Sud, 91405 Orsay Cedex, France.
** Corresponding author at: FOM-Institute for Plasma Physics Rijnhuizen, Edisonbaan 14, 3439MN Nieuwegein, The Netherlands. Tel.: +31 30 6096999; fax: +31 30 6031204.
E-mail addresses: olivier.pirali@synchrotron-soleil.fr (O. Pirali), joso@rijnhuizen.nl (J. Oomens).

1387-3806/$ – see front matter © 2010 Elsevier B.V. All rights reserved.
doi:10.1016/j.ijms.2010.05.018

Here, we consider the experimental infrared spectra of cationic diamondoid molecules. Based on computed optical properties, Bauschlicher et al. concluded that cationic species could also contribute to the observed emission signal [17]. These calculations indicate, however, that the band positions in the 3 μm spectral range are similar for neutral and cationic species. This makes it difficult to distinguish between neutral and ionic diamondoids in interstellar emission spectra. Indeed, to date only two bands at 3.43 μm and 3.53 μm have been suggested to be due to diamondoid species. For both the cations and the neutrals, these modes involve symmetric and antisymmetric hydrogen stretching motions of the CH_2 and CH groups on the edges and surfaces of the diamondoid molecules. All other IR active modes are about 10 times weaker than the CH stretching modes in neutral diamondoids, but this is not the case for their cations [17].

In addition, the photo-physical processes underlying the interstellar emission remain poorly understood. Similar to diamond crystals and unlike PAH molecules, diamondoids show very weak absorption bands in the UV spectral range [17], which are moreover close to their ionization potentials. Emission features arising from these molecular species are therefore expected to be observable only when the UV radiation field is intense, which suggests in turn that cationic species might be abundant in those regions.

We note further that the ionic forms of diamondoids, and especially their carbocation forms as studied in this work, are also well known as the intermediates in the synthesis of the lower diamondoids [3,18]. Moreover, they were shown to be important intermediates in the site-specific functionalization of diamondoid molecules [19].

Several spectroscopic studies of diamondoid species have been reported to determine their structures, see e.g., Filik et al. [20], who studied the Raman spectra of diamondoids as large as heptamantane. IR spectra have been obtained using attenuated total reflection (ATR) spectroscopy and compared with density functional theory (DFT) calculations at different levels of theory [21]. Gas-phase emission spectra of adamantane, diamantane and triamantane have been recorded in the 3 μm region using an experimental set-up described in Ref. [22]. Chiral properties of helical diamondoids have been evidenced by circular dichroism spectroscopy in the optical and infrared [23]. Recently, accurate ionization potentials of the first five diamondoid molecules (adamantane, diamantane, triamantane, tetramantane and pentamantane) in the gas phase have been obtained using VUV radiation from the Bessy synchrotron [24]. Several X-ray studies provided information on the HOMO–LUMO gap of diamondoid species [25], which is of interest for semiconductor research. Finally, various computational studies have investigated the properties of diamondoid molecules (see e.g., Refs. [17,26,27]).

Experimentally very little is known about the gas-phase structure and properties of cationic diamondoids. Polfer et al. [28] reported the IR spectrum of the gas-phase adamantyl cation ($C_{10}H_{15}^+$), i.e., the dehydrogenated adamantane cation, constituting the first experimental IR spectrum of a gas-phase cationic diamondoid species, which allowed to determine the structure of the most stable isomer. The hydrogen atom can be detached from two distinct C-atoms, giving rise to two isomeric structures for the adamantyl cation [26]. The IR spectrum showed good agreement with the calculated spectrum of the lowest energy isomer. Relative energies of the cationic species in solution have been studied because of their relevance in the synthesis of diamondoid molecules and their derivatives [19,29].

In this work, we record the infrared multiple photon dissociation (IRMPD) spectra of diamantyl and triamantyl cations using the experimental methods of Ref. [28]. We present a spectroscopic comparison of the infrared features of the neutral and carbocationic species.

2. Laboratory methods

2.1. Experiments

The IRMPD spectra of the diamantyl and triamantyl cations were recorded using the free electron laser FELIX [30] in a quadrupole ion trap coupled to a time-of-flight mass spectrometer (R.M. Jordan, California). This instrument has been used previously to record IRMPD spectra of several cationic polycyclic aromatic hydrocarbons (PAHs) and has been described in detail elsewhere [31]. The spectra presented here have been obtained applying experimental methods similar to those used to record the infrared spectrum of the adamantyl cation [28]. Here we give only a brief description.

Diamondoid molecules possess only very weak electronic absorption bands, which are moreover located at energies close to the ionization potential (IP) [17]. The IPs of the five smallest neutral diamondoid molecules have been experimentally determined [24] and the values for adamantane, diamantane and triamantane are 9.23 eV, 8.80 eV and 8.57 eV, respectively. Therefore, photoionization based on the absorption of two 193 nm photons from a ArF excimer laser, as used for PAH molecules, is inefficient for diamondoid systems. As used previously for adamantane [28], efficient ionization of diamondoids can be achieved via charge transfer (CT) from cationic species with a high ionization potential (IP). Benzoic acid is therefore vaporized together with the diamondoid molecule in the ion trap chamber, which produces abundant cationic UV photofragments [32,33] (in particular the benzoyl cation at *m/z* 105) with IPs higher than those of the diamondoid molecules under study. Storing the benzoyl cation in the trap for typically 100 ms produces abundant diamondoid ions by charge transfer ionization.

Diamantane and triamantane vapor are produced by placing the solid samples in an oven kept at a temperature of about 44 °C and 64 °C, respectively. All species lower in mass than the parent diamondoid (benzoic acid, its fragments and diamondoid fragments) are axially ejected from the trap by increasing the RF voltage for few ms. It is known that diamondoid cations may undergo rapid hydrogen atom loss leading to a stable closed-shell molecular species. We therefore expect to have isolated diamantyl and triamantyl cations rather than the diamantane and triamantane radical cations, although the mass resolution of the ion trap/TOF mass spectrometer is not sufficient to confirm this from the mass spectrum. However, analysis of the IRMPD spectra obtained confirms the identity of the ions as the dehydrogenated diamondoid cations, similar to what was observed for adamantane [28].

The mass-selected ion cloud is irradiated with the intense FELIX IR beam (see Ref. [30] for details on the FELIX free electron laser), which is sharply focused in the center of the quadrupole trap. When the wavelength of FELIX is in resonance with an IR active mode of the ion, multiple photon absorption occurs, mediated by intramolecular vibrational redistribution (IVR), which is very efficient for such large species. Tens to hundreds of IR photons are thus absorbed by a single molecule, raising its internal energy to above the dissociation threshold. Upon resonance, loss of CH, C_2H_4, C_3H_6 and C_4H_8 is observed using the TOF mass analyzer. Loss of C_2H_4 is the most abundant dissociation channel and the final IRMPD spectra of the parent molecules are obtained by co-adding the intensities of all photofragments as a function of wavelength of the FEL. The wavelength of the FEL is calibrated against a grating spectrometer and the relative fragmentation intensities are corrected for slowly decreasing FEL power towards short wavelengths. Because the spectra are obtained through multiple photon excitation, the experimental band centers are expected to be slightly red-shifted compared to a linear absorption experiment [31]. The shift depends on the (unknown) anharmonicity of the vibrational modes involved in the excitation process, but is usually on the order of less than 10 cm^{-1}.

IR spectra of the carbocations of adamantane, diamantane and triamantane are compared with those of the corresponding neutral molecules in the gas phase. To this end, the gas-phase spectrum of adamantane has been taken from the NIST webbook.[1] The 600–3100 cm^{-1} spectrum of gas-phase diamantane has been recorded here using an IFS125 Bruker interferometer. The vapor of room-temperature diamantane was leaked into a 150-m absorption pathlength cell (White type arrangement of the multipass optics). The cell has been baked several days before injecting the sample and the interferometer was continuously evacuated during spectrum acquisition to limit the intense absorption of water vapor lines. Because of its low vapor pressure at room temperature, we could not record the gas-phase spectrum of triamantane with the same technique. Therefore, the triamantyl cation spectrum is compared to the solid state spectrum of neutral triamantane recorded using attenuated total reflection (ATR) spectroscopy [21].

2.2. DFT calculations

The various isomeric structures of the diamantyl and triamantyl cations were optimized using density functional theory (DFT) computations as implemented in Gaussian03. All calculations employed the B3LYP functional and the 6-31G(d,p) basis set to optimize the structures and compute the IR spectra. Similar levels of theory have been successfully applied to similar-sized hydrocarbon species including diamondoids [20,21,29]. In addition, B3LYP calculations on the lowest energy isomer of the diamantyl carbocation show that increasing the basis set beyond 6-31G(d,p) does not lead to an appreciable change in the calculated vibrational spectrum (see Fig. S1 in the Supplementary Information). All carbocation structures are assumed to possess a closed-shell electronic structure. Calculated frequencies are scaled by 0.975 for the mid-IR vibrational modes and by 0.95 for the CH stretching modes to account for the different anharmonicities of these vibrational modes.

Computed spectra of the three isomers of the diamantyl cation are shown in Fig. 1. The three isomers (structures **D1**, **D2**, and **D3**) of the diamantyl cation arise from H-atom abstraction at three distinguishable sites. All secondary carbon atoms (i.e., CH_2 groups) are symmetrically equivalent in diamantane and H-abstraction from one of them forms isomer **D3**. There are two symmetrically distinguishable tertiary carbon atoms (i.e., CH groups) in diamantane: one where the tertiary C-atom is connected to three CH_2 groups (**D2**) and one where the tertiary C-atom is connected to two CHs and one CH_2 (**D1**). Calculations were also performed for the triamantyl cation, which possesses seven isomers: four isomers result from H-loss from a tertiary carbon and three isomers from H-loss from a secondary carbon. We note here that the relative energies found for the different tertiary carbon dehydrogenated isomers compare well to those reported previously in Ref. [19]. The structures of the isomers are shown in Fig. 2.

3. Spectra and structures

3.1. Energetics of H-atom loss

While the mass resolution of our ion trap/TOF mass spectrometer is insufficient to determine whether the parent ion is the diamondoid radical cation or the corresponding closed-shell dehydrogenated cation, the IR spectra (vide infra) strongly suggest that the dehydrogenated cation (carbocation) is formed in the experiment. This is similar to what has been observed in the experiments on ionized adamantane [28], where the resolution was just sufficient to observe the difference. In that paper, a rationale was given for why the adamantyl cation is observed rather than the adamantane radical cation and we believe that a similar reasoning applies here.

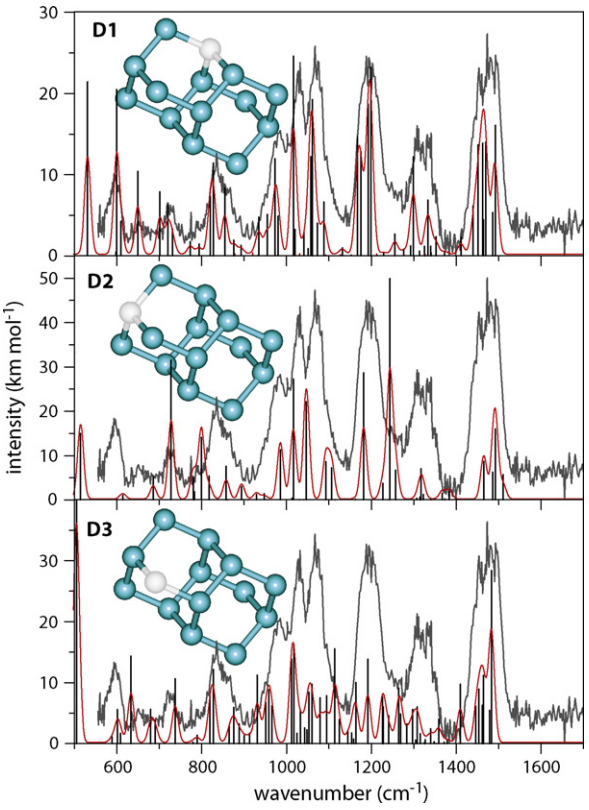

Fig. 1. IRMPD spectrum of the diamantyl cation (gray trace in all panels) compared with DFT calculated spectra for the three isomers of the diamantyl cation. The stick spectra (black) were convoluted with a 20 cm^{-1} Gaussian line shape (red trace). The isomeric structures are shown where the H-atom is abstracted from the highlighted C-atom and where all H-atoms have been omitted for clarity.

Aliphatic hydrocarbons have a narrow energy gap between ionization potential (IP) and appearance energy (AE) of the singly dehydrogenated cation. For instance, according to the NIST Chemistry Webbook, the difference AE – IP amounts to 1.1 eV for ethane and to only 0.6 eV for propane, while the IPs are on the order of 11 eV. For adamantane, the difference AE – IP was estimated to be around 1.4 eV [28]. Any excess energy deposited in a non-resonant ionization scheme, such as the chemical ionization used here (but also broadband VUV ionization as may occur in circumstellar environments), will thus likely result in the singly dehydrogenated ion (carbocation).

To further exclude the possibility that the radical cation diamondoid is responsible for the spectra observed instead of the carbocation, we compared the experimental spectra with computed spectra for the diamondoids in their radical cation form (see Fig. S2 in the Supplementary Information). The adamantane cation spectrum was calculated at the C_{3v} structure reported in Ref. [29]. Although their HOMOs are known to be non-degenerate [29], it was necessary to relax the symmetry of the diamantane and triamantane radical cations to C_s to mitigate difficulties in the SCF convergence and to remove imaginary frequencies. Fig. S2 clearly shows that no spectral match is found between the radical cation calculated spectra and the experimental data. In combination with the accurate mass determination for adamantane, the AE versus IP considerations given above, and the spectral match with the closed-shell carbocation structures (vide infra), this strongly suggests that

[1] webbook.nist.gov.

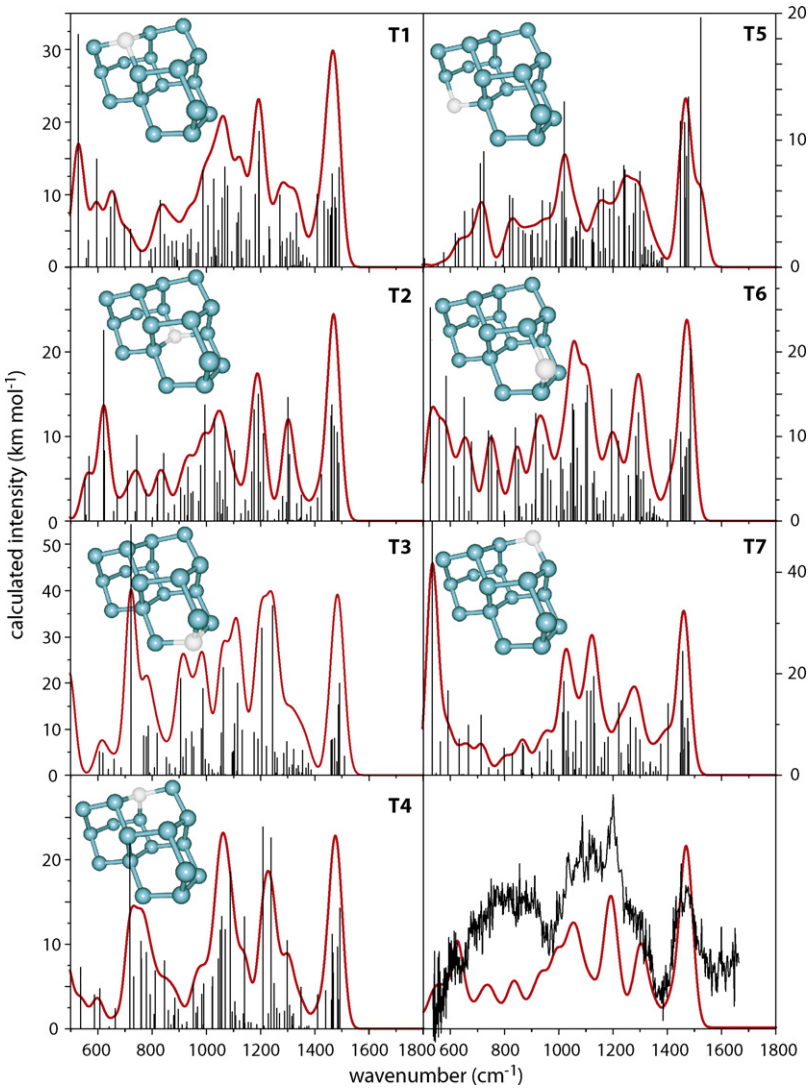

Fig. 2. Calculated IR spectra for the seven isomers of the triamantyl cation represented as stick spectra (black) and 30 cm^{-1} Gaussian line shape convolutions (red trace). The experimental IRMPD spectrum of the triamantyl cation is shown in the last panel together with the weighted average spectrum of the most stable isomers **T1** –**T4**. The structures are also shown, where the H-atom is abstracted from the highlighted C-atom and where all H-atoms have been omitted for clarity. (For interpretation of the references to color in this figure legend, the reader is referred to the web version of the article.)

the diamondoid ions are observed in their dehydrogenated form. This forms the basis for the discussion that follows.

3.2. IRMPD spectrum and structure of the diamantyl cation

The experimental IRMPD spectrum obtained using the diamantane sample is shown in Fig. 1. As was the case for the adamantyl cation [28] and for the reasons given in the previous section, we expect that the spectrum observed is that of the dehydrogenated diamantane cation, i.e., the diamantyl cation ($C_{14}H_{19}^+$), rather than that of the diamantane radical cation ($C_{14}H_{20}^+$). For the radical cation diamondoids, there is some doubt as to where the charge is localized [17], since there are several distinct C–C bonds which can be ionized (note that the charge is not delocalized as in PAHs). In the dehydrogenated diamondoid cations under study here, this is not the case: the charge is localized on the carbon atom where the H-atom is removed, forming a carbocation. However, there are multiple isomers for each of the dehydrogenated diamondoid cations, as there are distinct carbon atoms from which the H-atom can be abstracted. These isomers are classified as C1 or C2 type depending on whether the H-atom is removed from a tertiary (CH) or a secondary (CH_2) carbon, respectively.

While for adamantane, all CH moieties as well as all CH_2 moieties are equivalent based on symmetry arguments, this is not the case for diamantane. Here, two symmetrically distinct tertiary carbons exist, while all secondary carbon atoms are equivalent, which results in three isomers for the diamantyl cation, two of C1 type and one of C2 type. These isomers are labelled as **D1**, **D2** and **D3** and their structures are shown in Fig. 1, where all H-atoms have been omitted for clarity and the dehydrogenated C-atom is highlighted.

While the structural differences between the different isomers of the diamantyl cation may appear to be marginal, their calculated spectra present clear differences, which can be used to reliably assign the experimental spectrum. Fig. 1 compares the experimental IR spectrum with the calculated spectra of each of the three isomers. It is immediately seen that the match with isomer **D1** is much better than with any of the other isomers; Table 1 compares the experimental band centers with the band centers resulting from a convolution of the **D1** computed spectrum with a 20 cm^{-1} FWHM Gaussian band profile. Calculated frequencies for all isomers are tabulated in Supplementary Material. In the **D1** isomer of the diamantyl cation, the H-atom is lost from one of the six equivalent tertiary carbon atoms that form a 'belt' fusing the two diamondoid cages. For structure **D2**, where the H-atom is lost from one of the

Table 1
Observed and calculated band centers (in cm^{-1}) of the diamantyl cation.

DFT		IRMPD
Frequency [a]	IR int [b]	Frequency
601	23	594
650	10	653
703	8	726
722	8	726
824	17	842
853	8	842
936	5	–
974	16	984
1017	28	1029
1060	32	1069
1172	26	1196
1197	39	1196
1298	13	1312
1333	9	1335
1462	34	1474
1489	21	1474

[a] Scaled by 0.975.
[b] Units of km/mol.

two tertiary carbons at the apical positions of the molecule, the mismatch with the experimental spectrum is especially evident in the 1200–1400 and the 700–900 cm^{-1} regions. The calculated spectrum for **D3** exhibits bands roughly at the right frequencies, but with very different relative intensities, so that the match with the experimental spectrum is not nearly as good as for **D1**. The calculated relative energies for the three isomers as listed in Table 2 support the assignment of the IRMPD spectrum to **D1**, since isomers **D2** and **D3** are higher in energy than **D1** by 0.1 eV and 0.5 eV, respectively. In addition, from solution-phase reactivity studies, the belt position H-atoms are known to be more labile than the apical position H-atoms [18].

The assignment to structure **D1** is analogous to that identified for the adamantyl cation previously [26,28] using IRMPD spectroscopy and DFT calculations, respectively. There it was concluded that H-atom loss to form the closed-shell carbocation occurs preferentially from a tertiary carbon, rather than from a secondary carbon. In general, calculations predict that in the gas phase the tertiary carbocations are more stable than the secondary ones by typically 0.5 eV.

Table 2
Relative electronic energies for the different isomers of the adamantyl, diamantyl and triamantyl cations at the B3LYP/6-31G(d,p) level of theory.

#	Sym	C1/C2 [a]	ΔE	
			eV	kJ/mol
Adamantyl cation ($C_{10}H_{15}^+$)				
A1	C_{3v}	C1	0	0
A2	C_s	C2	0.492	47.5
Diamantyl cation ($C_{14}H_{19}^+$)				
D1	C_s	C1	0	0
D2	C_{3v}	C1	0.133	12.8
D3	C_1	C2	0.511	49.3
Triamantyl cation ($C_{18}H_{23}^+$)				
T2	C_s	C1	0	0
T1	C_1	C1	0.037	3.6
T4	C_s	C1	0.103	10.0
T3	C_s	C1	0.138	13.3
T5	C_1	C2	0.490	47.3
T7	C_s	C2	0.526	50.8
T6	C_1	C2	0.576	55.6

[a] C1/C2: H-loss from tertiary/secondary C-atom.

3.3. IRMPD spectrum and isomeric structure of the triamantyl cation

Given our observations for adamantane [28] and diamantane, it is likely that ionization of triamantane is accompanied by rapid H-atom loss resulting in the closed-shell triamantyl cation ($C_{18}H_{23}^+$). Not unexpectedly, the situation becomes more complicated for the triamantyl ion, as seven distinct isomers of the triamantyl cation exist (see Fig. 2). Four isomers are obtained by H-atom loss from a tertiary carbon atom (C1 type isomers) and three by H-atom loss from a secondary carbon atom (C2 type isomers). The four C1 type isomers (labelled **T1** –**T4**) have energies within 0.1 eV of each other, while all C2 type isomers (isomers **T5** –**T7**) are less stable by around 0.5 eV (see Table 2). This energy difference is thus analogous to that found for C1 and C2 type isomers of the adamantyl and diamantyl cations. Of the C1 isomers, **T1** and **T2** are computed to be substantially more stable than **T3** and **T4**. Although the ions in the trap are not necessarily in thermodynamic equilibrium, a simple Boltzmann distribution at the temperature of the oven would yield a population of **T1** around 30% of that in **T2**, while the population of **T3** and **T4** would be less than 3%.

The experimental spectrum recorded for the triamantyl cation shown in the lower right panel of Fig. 2 displays fairly broad and partly unresolved features. DFT calculated energies for the seven isomers are listed in Table 2 and their spectra are shown in the separate panels of Fig. 2. The increased molecular complexity and the low symmetry of the systems give rise to congested spectra, as can be appreciated from the stick spectra. The solid red lines represent 30 cm^{-1} FWHM Gaussian convolutions of the stick spectra. These congested spectra, in combination with a possible mixture of isomers and the higher temperature of the oven are believed to give rise to the fairly unresolved spectrum observed for this species.

In the last panel, the experimental IRMPD spectrum is compared with a Boltzmann-weighted sum of the spectra of the C1 type isomers **T1** –**T4**. Despite the low experimental resolution obtained, the features near 1465 and 1195 cm^{-1} appear to be well reproduced by theory. In addition, the shoulder around 1290 cm^{-1} and the broad feature extending from 1000 to 1200 cm^{-1} appear to have a reasonable counterpart in the convoluted theoretical spectra. On the other hand, towards the long wavelength end of the spectrum, the experiment shows more absorption than the convoluted theoretical spectra. Perhaps a higher-than-thermal abundance of isomers **T3** and **T4** gives rise to this increased absorption. In conclusion, while the present spectrum does not allow to truly identify the contributing isomers, the spectrum shows features that appear to be typical of diamondoid carbocations, as will be discussed further below.

4. Spectral analysis

The IR spectra of dehydrogenated cationic diamondoids recorded here are compared to their neutral diamondoid counterparts. The three cation spectra are also compared to each other to reveal spectral characteristics for this class of cationic species.

4.1. IR spectra of adamantane and the adamantyl cation

Fig. 3 compares the gas-phase spectra of neutral adamantane (taken from the NIST Chemistry Webbook) and cationic adamantyl (taken from Ref. [28]) along with their DFT calculated spectra. The calculated spectrum of neutral adamantane reproduces the experimental one reasonably well. Small differences in terms of both frequencies and relative intensities are observed for the 3 μm stretching modes, which may be due to strong anharmonic couplings between these modes not accounted for in the calculations

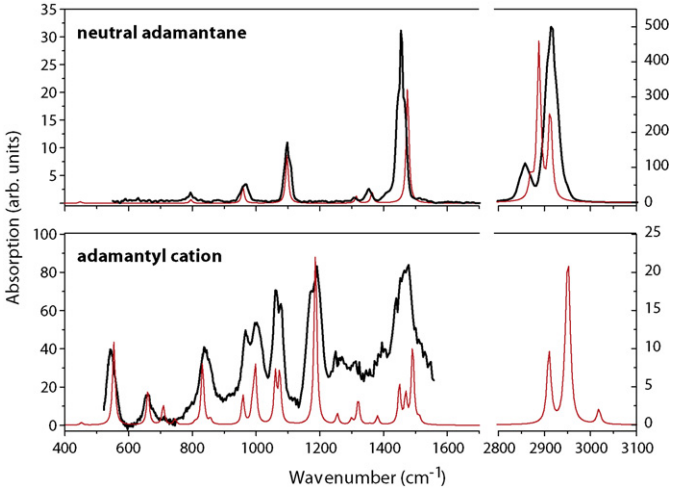

Fig. 3. Comparison of the experimental (from NIST Chemistry WebBook) and calculated spectra of neutral adamantane (upper panel) with the IRMPD and calculated spectra of adamantyl cation (lower panel). Note the very different scales on the ordinates of the spectra.

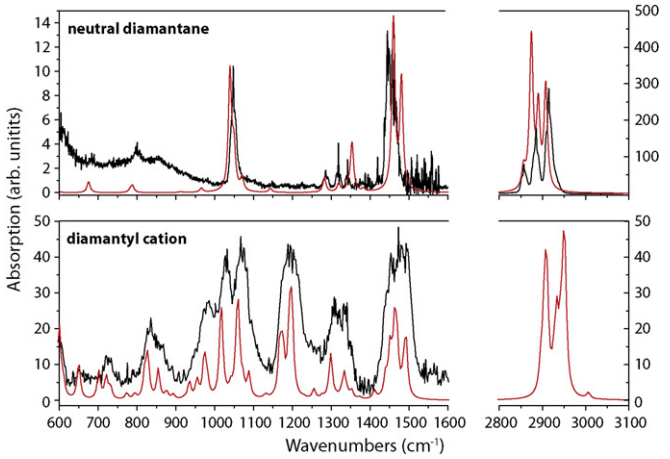

Fig. 4. Comparison of the gas-phase absorption spectrum of neutral diamantane and the IRMPD spectrum of the diamantyl cation. The sharp features in the 1500–1600 cm^{-1} range of the spectrum of neutral diamantane are due to residual water vapor in the absorption cell. Calculated spectra for both species are shown along with the experimental spectra.

[16]. In addition, the frequency of the CH_2 scissor mode (ν_{23}) near 1450 cm^{-1} is substantially overestimated by the DFT calculation; similar shifts for this particular vibration were observed in the IR spectra of a series of higher diamondoids [21].

Due to its lower symmetry, the adamantyl cation (C_{3v}) shows a higher density of IR active transitions than neutral adamantane (T_d). Nonetheless, the CH_2 scissor mode observed around 1450 cm^{-1} is recognized in both species. Also, the CH_2 rocking modes located near 1100 cm^{-1} and C–C stretching modes near 950–1000 cm^{-1} are found in the same spectral region.

On the other hand, one notices large differences in the intensities of the CH stretching modes relative to the other mid-IR modes in the spectra of the two species. This is best appreciated when comparing the scales on the ordinates of the graphs in Fig. 3. Going from the neutral to the cationic system, the calculated intensities of the mid-IR modes increase by a factor of around 2–5, but the CH stretching modes are calculated to become 20–50 times weaker. In the calculated spectra, the most prominent peak of the 3 μm region is shifted towards higher frequencies by less than 50 cm^{-1}. Another striking difference between the adamantyl and adamantane spectra concerns the band located near 1200 cm^{-1}, which is due to CH_2 bending vibrations; this band appears as strong as the CH_2 scissor modes for the adamantyl cation, but is completely absent in the neutral adamantane spectrum. Similarly in the low frequency region, the cage deformation modes located at frequencies lower than 900 cm^{-1} appear to be especially sensitive to the structure changes between adamantane and the adamantyl cation. For example, the band located near 800 cm^{-1} in the neutral spectrum is blue-shifted by about 50 cm^{-1} for the adamantyl cation. A strong enhancement of intensity is also observed here.

4.2. IR spectra of diamantane and the diamantyl cation

The gas-phase spectra of neutral diamantane and the diamantyl cation are compared in Fig. 4. The calculated spectrum of neutral diamantane is in relatively good agreement with the experimental gas-phase spectrum. Some residual water vapor lines due to the ν_2 bending mode are observed in the 1500–1600 cm^{-1} region. As for adamantane, the calculated frequencies of the CH stretching modes around 2900 cm^{-1} match the experimental bands relatively well, while the relative intensities are not well predicted. As for adamantane, strong anharmonic couplings between the closely spaced CH stretching modes of equal symmetry may compromise the results of the harmonic frequency calculations somewhat.

In the mid-IR region, the calculations reproduce the gas-phase spectrum of neutral diamantane reasonably well, both in terms of frequencies and intensities (note that the rising background $< 1000\ cm^{-1}$ is an experimental artefact). This is somewhat in contrast with the ATR spectrum of diamantane published recently [21], where the relative intensities of several mid-IR modes showed large differences in comparison with the DFT calculations. Particularly in the 1300–1400 cm^{-1} spectral range, the CH bending modes showed intensities which were about 10 times larger in the ATR spectrum than in the computed spectrum (and in the current in the gas-phase spectrum). Also the lower-frequency bands assigned to deformation modes of the carbon frame and C–C stretching modes (at about 650 cm^{-1}, 850 cm^{-1} and 950 cm^{-1}) are hardly observable in the gas-phase spectrum, as predicted by DFT, while they were strong bands in the ATR spectrum. We ascribe these discrepancies to unknown matrix effects in the ATR experiments.

The main differences between the gas-phase spectra of diamantane and the diamantyl cation are similar to those observed for the adamantane versus adamantyl cation spectra. In the 3 μm region, the vibrational bands of the diamantyl cation are calculated to appear at slightly higher frequencies (shift of about 50 cm^{-1}) with an intensity that is around 10 times lower than that of neutral diamantane.

In the 600–1600 cm^{-1} spectral range, the intensities of the dehydrogenated cation bands are more intense than for neutral diamantane. The intense 1200 cm^{-1} band of the diamantyl cation, which is mainly due to a CH/CH_2 bending mode is as intense as the CH_2 scissoring modes between 1400 cm^{-1} and 1500 cm^{-1}, while no band is observed here in the neutral diamantane spectrum. As for the adamantane versus adamantyl cation comparison, the low frequency part of the spectrum shows large differences. The 800 cm^{-1} deformation modes of the neutral are shifted by about 50 cm^{-1} as compared to the calculated and experimental spectra of the diamantyl cation. An intense mode centered at 600 cm^{-1} observed in the diamantyl cation spectrum is absent from the neutral diamantane spectrum.

4.3. IR spectra of triamantane and the triamantyl cation

Due to the low vapor pressure of triamantane, a gas-phase absorption spectrum of the neutral species could not be obtained

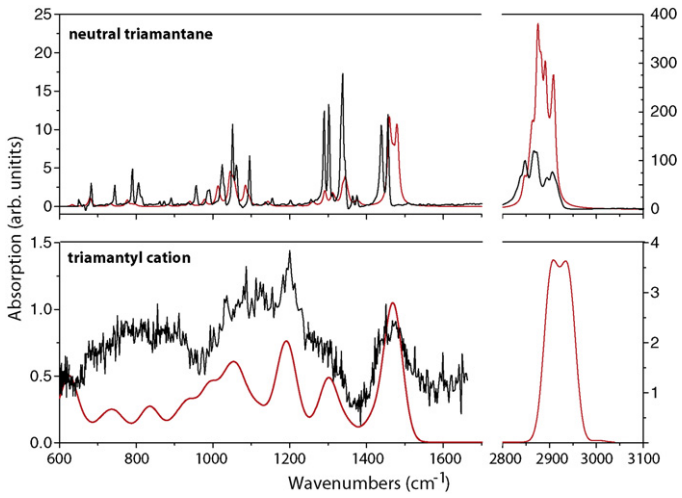

Fig. 5. Comparison of the experimental and calculated spectra of neutral triamantane (upper panel) and triamantyl cation (lower panel).

and hence, Fig. 5 shows the neutral triamantane ATR spectrum from Ref. [21] together with the calculated DFT spectrum. The relative intensities of several mid-IR modes are observed to be substantially higher than in the DFT calculated spectrum and we assume that this is again an artefact of the condensed-phase nature of the ATR method, as was clearly demonstrated for diamantane. The gas-phase IRMPD spectrum of the triamantyl cation spectrum is reproduced in the lower panel of Fig. 5. Because of the rather unresolved appearance of the IRMPD spectrum, a detailed comparison with the neutral triamantane spectrum cannot be performed. Nevertheless, the trends observed in the spectral comparisons of adamantane versus the adamantyl cation and diamantane versus the diamantyl cation appear to be similar here.

Several mid-IR modes have the same frequencies and intensities in the neutral and dehydrogenated cation spectra. The scissoring modes of the triamantyl cation are observed in the 1500 cm^{-1} spectral region in the broad IRMPD spectrum. The CH bending modes around 1300 cm^{-1} are also distinguishable in the IRMPD spectrum and fall around the same frequency as in neutral triamantane. The spectral information that can be extracted from the 1000–1300 cm^{-1} range is limited as a consequence of the unresolved nature of the IRMPD spectrum, but we assume that absorption in the 1000–1100 cm^{-1} range is due to the C–C stretching modes.

The intense band centered around 1200 cm^{-1}, which appears to be a diagnostic feature for the dehydrogenated cationic diamondoid molecules, is also present in the triamantyl cation spectrum. Again, this band is missing in the spectrum of neutral triamantane.

As for the smaller diamondoids investigated here, the 3 μm bands are calculated to be much weaker in the triamantyl cation spectrum than in the neutral spectrum.

4.4. General features in the cationic diamondoid spectra

Comparison of all three cationic spectra in Fig. 6 now provides an opportunity to identify absorption bands characteristic for this class of cationic species, so that they could eventually be searched for in interstellar spectra. The CH stretching modes in the 3 μm spectral range are not good candidates because these bands are weak and, more importantly, overlap severely with the CH stretching bands in the corresponding neutral diamondoids. In general, the band positions in the adamantyl and diamantyl cation spectra between 800 cm^{-1} and 1600 cm^{-1} are very similar forming an interesting fingerprint for this class of cationic hydrocarbons. From

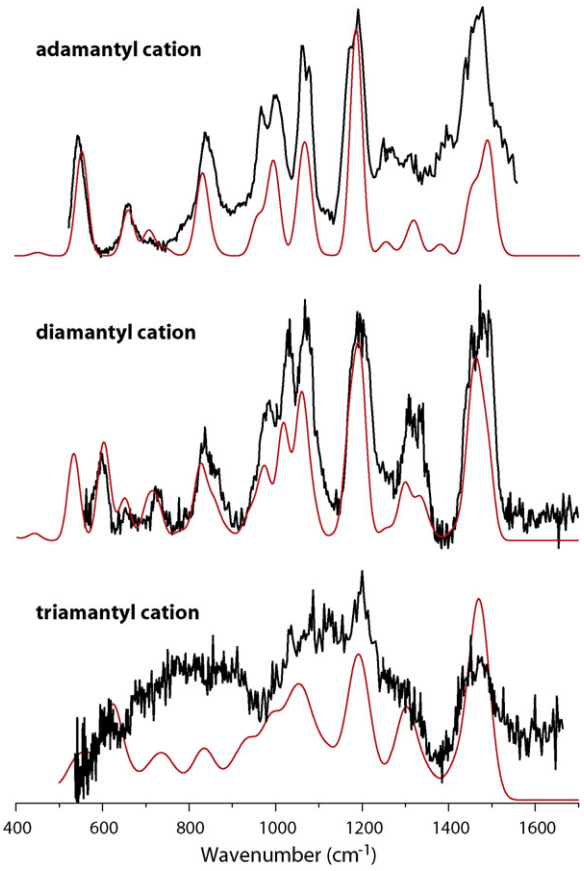

Fig. 6. Comparison of the gas-phase IR spectra of the three cationic diamondoid species adamantyl, diamantyl and triamantyl.

the main infrared features of the triamantyl cation near 1195 cm^{-1} and 1465 cm^{-1}, its spectrum also appears similar, although clearly the resolution deteriorates as the systems increase in size, which is likely caused by the increasing spectral congestion. The intense band centered at 1200 cm^{-1} appears to be particularly characteristic in the spectra of the dehydrogenated cationic diamondoids and could be used to distinguish these species from their neutral counterparts. Note, however, that this band located at 8.33 μm falls close to two intense features in the emission spectra of PAHs at 7.8 μm and 8.6 μm. Differences in the spectra of the different cationic diamondoids are mainly found in the far-IR range below 800 cm^{-1}, where the absorption bands observed are primarily due to cage deformation modes. These modes are generally very delocalized over the molecules and it stands to reason that they would be different for differently sized members of the same class of species. Moreover, comparison with the neutral diamondoid spectra shows that these modes are also sensitive to the change in structure between neutral and carbocationic species.

5. Conclusions

Experiments employing chemical ionization of neutral diamondoid molecules indicate that ionization is accompanied by facile H-atom loss, leading to more stable closed-shell carbocations. This observation can be rationalized based on the close proximity of the ionization potential and the appearance energy of the singly dehydrogenated ion. One could imagine that this process might also play a role in UV dominated regions of the interstellar medium (ISM), where ionized diamondoid species, if present, occur as closed-shell dehydrogenated species rather than as radical cation species.

IRMPD spectra were recorded for cationic diamantyl and triamantyl in the 500–1600 cm^{-1} spectral range. Comparing our IRMPD spectra with DFT calculations permitted to identify the structures of the most favored isomers for the diamantyl and triamantyl cations. As shown for the adamantyl cation [26,28], the H-atom abstraction occurs preferentially on a tertiary carbon atom (CH) rather than on a secondary carbon atom (CH_2), which is also supported by the calculated relative energies of each of the isomers and moreover relates to the behavior in functionalization reactions of diamondoid molecules in solution [19]. Of the two isomers of tertiary carbocationic diamantyl, the IR spectrum identifies the lowest energy isomer as being present experimentally. In this isomer, the H-atom is abstracted from one of the 'belt' tertiary carbon atoms rather than from one of the apical carbon atoms, again in line with solution-phase chemistry [18,19].

The DFT calculations also provide an assignment for most of the observed vibrational bands of the diamondoidyl cations. As described in Ref. [17], cationic forms of diamond-like molecules may contribute to the observed 3.43 μm and 3.53 μm emission bands, although the bands at these wavelengths are likely dominated by neutral diamondoids. Hence, we compared in particular the IR signature in the 6–16 μm range for the neutral and carbocationic forms of adamantane, diamantane and triamantane as the simplest members of the diamondoid family. Substantial spectral differences exist in terms of relative intensities of the IR modes. The calculations suggest that the intensities of the CH stretch modes in the 3 μm region become more than 10 times weaker in the dehydrogenated cationic species as compared to the neutrals, similar to what has been reported for radical cation diamondoids, based on calculated spectra of several higher diamondoid species [17]. The bands in the mid-IR range on the other hand, become substantially more intense upon going from the neutral to the cationic species. Overall, this reversal of relative intensities between the 3 μm and mid-IR ranges is similar to what is observed for polycyclic aromatic hydrocarbon (PAH) molecules [34,35]. Finally, in this context, it is also of interest to note that the neutral diamondoid relative band intensities in the mid-IR range as calculated by DFT are well reproduced by the gas-phase diamantane spectrum recorded here, in contrast to previously recorded condensed-phase ATR spectra [21].

Acknowledgement

This work is part of the research program of FOM (contract 03PR2218), which is financially supported by the Nederlandse Organisatie voor Wetenschappelijk Onderzoek (NWO). We gratefully acknowledge the excellent support by Lex van der Meer, Britta Redlich and others at the FELIX staff.

Appendix A. Supplementary Data

Supplementary data associated with this article can be found, in the online version, at doi:10.1016/j.ijms.2010.05.018.

References

[1] V. Prelog, R. Seiwerth, Uber die synthese des adamantans, Ber. deutsch. chem. Gesell. 74 (1941) 1644–1648.
[2] P.V.R. Schleyer, A simple preparation of adamantane, J. Am. Chem. Soc. 79 (1957) 3292–13292.
[3] O. Farooq, S. Morteza, F. Farnia, M. Stephenson, G. Olah, Superacid-catalyzed near quantitative isomerization of $C_{4n+6}H_{4n+12}$ (n = 1–3), J. Org. Chem. 53 (1988) 2840–2843.
[4] D. Fărcaşiu, H. Bohm, P.V.R. Schleyer, Stepwise elaboration of diamondoid hydrocarbons. Synthesis of diamantane from adamantane, J. Org. Chem. 42 (1977) 96–102.
[5] E. Osawa, A. Furusaki, N. Hashiba, T. Matsumoto, V. Singh, Y. Tahara, E. Wiskott, M. Farcasiu, T. Iizuka, N. Tanaka, T. Kan, P.V.R. Schleyer, Thermodynamic rearrangements of larger polycyclic hydrocarbons derived from the 38.5 and 41.5° C melting dimers of cyclooctatetraene, J. Org. Chem. 45 (1980) 2985–2995.
[6] J.E. Dahl, S.G. Liu, R.M.K. Carlson, Isolation and structure of higher diamondoids, nanometer-sized diamond molecules, Science 299 (2003) 96–99.
[7] R. Lin, Z.A. Wilk, Natural occurrence of tetramantane ($C_{22}H_{28}$), pentamantane ($C_{26}H_{32}$) and hexamantane ($C_{30}H_{36}$) in a deep petroleum reservoir, Fuel 74 (1995) 1512–1521.
[8] W.C. Saslaw, J.E. Gaustad, Interstellar dust and diamonds, Nature 221 (1969) 160.
[9] R.S. Lewis, T. Ming, J.F. Wacker, E. Anders, E. Steel, Interstellar diamonds in meteorites, Nature 326 (1987) 160–162.
[10] O. Guillois, G. Ledoux, C. Reynaud, Diamond infrared emission bands in circumstellar media, Astrophys. J. 521 (1999) L133–L136.
[11] T.Y. Brooke, K. Sellgren, R.G. Smith, A study of absorption feature in the 3 micron spectra of molecular cloud sources with H_2O ice bands, Astrophys. J. 459 (1996) 209–215.
[12] E. Dartois, L. d'Hendecourt, Search for NH_3 ice in cold dust envelopes around YSOs, Astron. Astrophys. 365 (2001) 144–156.
[13] C.F. Chen, C.C. Wu, C.L. Cheng, S.Y. Sheu, H.C. Chang, The size of interstellar nanodiamonds revealed by infrared spectra of CH on synthetic diamond nanocrystal surfaces, J. Chem. Phys. 116 (2002) 1211–1214.
[14] Y.R. Chen, H.C. Chang, C.L. Cheng, C.C. Wang, J.C. Jiang, Size dependence of CH stretching features on diamond nanocrystal surfaces: infrared spectroscopy and density functional theory calculations, J. Chem. Phys. 119 (2003) 10626–10632.
[15] A.P. Jones, L.B. D'Hendecourt, S.-Y. Sheu, H.-C. Chang, C.-L. Cheng, H.G.M. Hill, Surface CH stretching features on meteoric nanodiamonds, Astron. Astrophys. 416 (2004) 235–241.
[16] O. Pirali, M. Vervloet, J.E. Dahl, R.M.K. Carlson, A.G.G.M. Tielens, J. Oomens, Infrared spectroscopy of diamondoid molecules: new insights into the presence of nanodiamonds in the interstellar medium, Astrophys. J. 661 (2007) 919–925.
[17] C.W. Bauschlicher, Y.F. Liu, A. Ricca, A.L. Mattioda, L.J. Allamandola, Electronic and vibrational spectroscopy of diamondoids and the interstellar infrared bands between 3.35 and 3.55 μm, Astrophys. J. 671 (2007) 458–469.
[18] G.A. Olah, G.K.S. Prakash, J.G. Shih, V.V. Krishnamurthy, G.D. Mateescu, G. Liang, G. Sipos, V. Buss, T.M. Gund, P.V.R. Schleyer, Bridgehead adamantyl, diamantyl, and related cations and dications, J. Am. Chem. Soc. 107 (1985) 2764–2772.
[19] A.A. Fokin, B.A. Tkachenko, P.A. Gunchenko, D.V. Gusev, P.R. Schreiner, Functionalized nanodiamonds. Part I. An experimental assessment of diamantane and computational predictions for higher diamondoids, Chem. Eur. J. 11 (2005) 7091–7101.
[20] J. Filik, J.N. Harvey, N.L. Allan, P.W. May, J.E.P. Dahl, S.G. Liu, R.M.K. Carlson, Raman spectroscopy of diamondoids, Spectrochim. Acta A 64 (2006) 681–692.
[21] J. Oomens, N. Polfer, O. Pirali, Y. Ueno, R. Maboudian, P.W. May, J.J. Filik, J.E. Dahl, S.G. Liu, R.M.K. Carlson, Infrared spectroscopic investigation of higher diamondoids, J. Mol. Spectrosc. 238 (2006) 158–167.
[22] O. Pirali, M. Vervloet, Far-infrared fourier transform emission spectroscopy in the gas phase, Chem. Phys. Lett. 423 (2006) 376–381.
[23] P.R. Schreiner, A.A. Fokin, H.P. Reisenauer, B.A. Tkachenko, E. Vass, M.M. Olmstead, D. Bläser, R. Boese, J.E.P. Dahl, R.M.K. Carlson, [123]Tetramantane: parent of a new family of σ-helicenes, J. Am. Chem. Soc. 131 (2009) 11292–11293.
[24] K. Lenzke, L. Landt, M. Hoener, H. Thomas, J.E. Dahl, S.G. Liu, R.M.K. Carlson, T. Möller, C. Bostedt, Experimental determination of the ionization potentials of the first five members of the nanodiamond series, J. Chem. Phys. 127 (2007) 084320.
[25] T.M. Willey, C. Bostedt, T. van Buuren, J.E.P. Dahl, S.G. Liu, R.M.K. Carlson, R.W. Meulenberg, E.J. Nelson, L.J. Terminello, Observation of quantum confinement in the occupied states of diamond clusters, Phys. Rev. B 74 (2006) 205432.
[26] G. Yan, N.R. Brinkmann, H.F. Schaefer III, Energetics and structures of adamantane and the 1- and 2-adamantyl radicals, cations, and anions, J. Phys. Chem. A 107 (2003) 9479–9485.
[27] J. Filik, J.N. Harvey, N.L. Allan, P.W. May, J.E.P. Dahl, S. Liu, R.M.K. Carlson, Raman spectroscopy of nanocrystalline diamond: an ab initio approach, Phys. Rev. B 74 (2006) 035423.
[28] N.C. Polfer, B.G. Sartakov, J. Oomens, The infrared spectrum of the adamantyl cation, Chem. Phys. Lett. 400 (2004) 201–205.
[29] A.A. Fokin, P.R. Schreiner, P. Gunchenko, S.A. Peleschanko, T.E. Shubina, S.D. Isaev, P.V. Tarasenko, N.I. Kulik, H.M. Schiebel, A.G. Yurchenko, Oxidative single-electron transfer activation of σ-bonds in aliphatic halogenation reactions, J. Am. Chem. Soc. 122 (2000) 7317–7326.
[30] D. Oepts, A.F.G. van der Meer, P.W. van Amersfoort, The free-electron-laser user facility FELIX, Infrared Phys. Technol. 36 (1995) 297–308.
[31] J. Oomens, A.G.G.M. Tielens, B.G. Sartakov, G. von Helden, G. Meijer, Laboratory infrared spectroscopy of cationic polycyclic aromatic hydrocarbon molecules, Astrophys. J. 591 (2003) 968–985.
[32] J. Oomens, J.M. Bakker, B.G. Sartakov, G. Meijer, G. von Helden, The infrared spectrum of the benzoyl cation, Chem. Phys. Lett. 367 (2003) 576–580.
[33] J. Oomens, G. von Helden, G. Meijer, Infrared photodissociation spectroscopy of the benzoic acid radical cation in a quadrupole trap, J. Phys. Chem. A 108 (2004) 8273–8278.
[34] F. Pauzat, D. Talbi, M.D. Miller, D.J. DeFrees, Y. Ellinger, Theoretical IR spectrum of ionized naphthalene, J. Phys. Chem. 96 (1992) 7882–7886.
[35] J. Szczepanski, M. Vala, Infrared frequencies and intensities for astrophysically important polycyclic aromatic hydrocarbon cations, Astrophys. J. 414 (1993) 646–655.